ACS OMEGA

Article

Cite This: ACS Omega 2019, 4, 8122−8135

http://pubs.acs.org/journal/acsodf

Single-Emulsion P(HB-HV) Microsphere Preparation Tuned by Copolymer Molar Mass and Additive Interaction

Neife Lilian Zalloum,[†,§] Geovany Albino de Souza,[‡] and Tatiana Duque Martins*[,‡]

[†]Chemistry Institute, State University of Campinas, P.O. Box 6154, 13083-971 Campinas, São Paulo, Brazil

[‡]Chemistry Institute, Federal University of Goiás, 74690-900 Goiânia, Goiás, Brazil

Supporting Information

ABSTRACT: Herein, we describe the production of poly(hydroxybutyrate-*co*-hydroxyvalerate) [P(HB-HV)]-based microspheres containing coumarin-6 (C6) or pyrene (Py) fluorophores as additives and models for hydrophobic and hydrophilic drug encapsulation. Their photophysical and morphological properties, as well as encapsulation efficiencies, are studied as this work aims to describe the influence of additive hydrophobicity/hydrophilicity on microparticle formation. These properties were studied by scanning electron microscopy, fluorescence confocal laser scanning microscopy (FCLSM), and steady-state fluorescence spectroscopy. The results show that the surfactant concentration, polymer molar mass, emulsification stirring rate, and the presence of the fluorophore and its nature are determinants of the P(HB-HV) microsphere properties. Also, encapsulation efficiency is shown to be governed by synergic effects of these parameters on the formation of microspheres. Moreover, size distribution is proved to be strongly influenced by the surfactant poly(vinyl alcohol) content. FCLSM showed that the fluorophores were efficiently encapsulated in P(HB-HV) microspheres at distinct distributions within the copolymer matrix. Surprisingly, nanospheres were observed in the microsphere surface, suggesting that microspheres are formed from nanosphere coalescence.

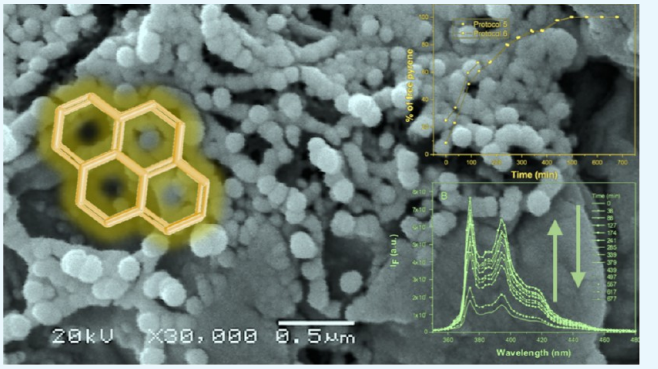

1. INTRODUCTION

Biodegradable polymer microspheres have been extensively investigated as potential carriers for drugs,[1−4] cosmetic products,[5−7] delivery systems, and for diagnostic purposes because of their biocompatibility, biodegradability, stability, and sustained-release properties.[8,9] Among the most studied materials for encapsulation are derivatives of poly(D,L-lactide), poly(D,L-lactide-*co*-glycolide) (PLGA), and poly-ε-caprolactones,[10] and the most widespread mechanism for encapsulation with them is the total enfold of the molecule of interest by the polymeric thin film to generate a spherical microparticle.

Among the polymers that can produce microspheres, poly(hydroxybutyrate) (PHB) and its copolymer with hydroxyvalerate (P(HB-HV)) have attracted the scientific interest, especially in biomedical field, because of its unique tunable mechanical properties, biocompatibility, and biodegradability.[11,12] These polymers, obtained from natural raw materials,[13,14] are considered green polymers, as they belong to the family of bacterial storage polyesters, which is another reason for their growing application.[15−17]

Drug delivery efficiency of these polymers can be controlled by tuning the polymer properties upon structure modification, for instance. With this regard, sulfamethizole-containing P(HB-HV) microparticles have presented slower drug release rates than PHB homopolymer-based microparticles[18] and distinct profiles, upon microparticles produced from P(HB-HV) of distinct HV contents.[19−21]

Delivery systems consisting of biodegradable polymer spheres[22−31] are interesting because they present several special characteristics, such as high surface-to-volume ratio, low density, and low coefficient of thermal expansion, which enable an efficient encapsulation and time-controlled drug release.[32] With this respect, it is important to ensure the internal and external morphology control of the microspheres, as they can influence the interaction with both the encapsulated drug and the microenvironment after the drug delivery. For this purpose, particles can be prepared by several methods, including oil/water emulsion and drying by solvent evaporation.[14,33−35] Although not new, emulsion techniques are very convenient to prepare microspheres, when a single emulsion is employed, or microcapsules, when double emulsions are employed. Both can encapsulate hydrophobic compounds, therefore, most drugs and chemical compounds.[36−40] Poly(vinyl alcohol) (PVA) is the most common emulsion stabilizer to achieve polymeric nano- and microparticles of PLGA, PHB, and P(HB-HV), allowing the

Received: March 25, 2019
Accepted: April 25, 2019
Published: May 3, 2019

preparation of small-sized particles with uniform diameter distribution.[41] Emulsifier identity and concentration play important roles in the physical−chemical and pharmaceutical properties of polymeric microspheres, including encapsulation efficiency, size and morphology, size distribution, surface chemistry and hydrophobicity, capture efficiency of the microparticles by macrophages, zeta-potential (ζ-potential), and release profile.[42] Changes in the surface properties have also been used as a strategy to obtain a controlled and sustained release of fluorescent probes.[43−46]

Regarding the release kinetics and efficiency, the control over the polydispersity in the size and morphology of the nano-/microsphere is indispensable to optimize the rates of particle degradation, drug stability, and release kinetics.[47,48] It has been demonstrated that smaller particles present higher release rates because of the shorter diffusion paths promoted by the higher surface/volume ratio.[45,49]

Nevertheless, for some applications, biocompatible and biodegradable nanoparticles are needed.[50−53] For instance, Eke et al.[54] conducted a study in which they compared the in vitro and transdermal penetration of PHB biodegradable micro-/nanoparticles. They showed that the size distribution of nanospheres is more uniform and that skin penetration and cellular uptake efficiency are the best for nanoparticles up to 500 nm,[54] whereas microspheres were not able to penetrate cell membranes. The spheres were produced by the oil-in-water method, which is similar to our approach, and the stirring rates were also controlled to obtain spheres of distinct sizes.[54] Mekala & Rajendran[55] also synthesized PHB nanospheres containing the drug ampicillin by the method of interfacial deposition, in which the drug in a water-miscible organic solvent is mixed with an aqueous solution of an emulsifier, leading to nucleation and growth of drug particles stabilized by the emulsifier.[52]

Among the techniques employed by researchers to characterize microparticles, fluorescence confocal laser scanning microscopy (FCLSM) has been widely applied to identify several structures as it enables to explore distinctively the surface and the inner portion of a particle.[56−63]

In this work, to attain more reliable microsphere formulation parameters and to comprehend the effect additives of distinct hydrophobicity may have on the microsphere formation, we prepared poly(hydroxybutyrate-*co*-hydroxyvalerate) P(HB-HV) microspheres by the water−oil emulsion technique[64] and, by steady-state fluorescence spectroscopy and by FCLSM, we determined the encapsulation efficiencies of the selected fluorophores, the polar coumarin-6 (C6) and the nonpolar pyrene (Py), which were used in this work as models for hydrophobic and hydrophilic drug encapsulation. Particle sizes, size distribution, and the effect of the use of these fluorophores as additives on the microsphere structures were evaluated by steady-state fluorescence spectroscopy, scanning electron microscopy (SEM), and ζ-potential measurements. Also, the controlled release of the fluorophores from the microspheres produced via distinct protocols was studied by steady-state fluorescence spectroscopy, and FCLSM was applied as a tool to evaluate fluorophore entrapment within microspheres.

2. RESULTS AND DISCUSSION

2.1. Microsphere Production and Characterization. P(HB-HV) microspheres containing fluorophores and microspheres without fluorophores were produced by mixing P(HB-HV) of two distinct molar masses (130 and 450 kg mol^{-1}) to a PVA emulsifier in a 1.0% w/v content, and the role of the P(HB-HV) copolymer molar mass on the size and size distribution of the produced microspheres was evaluated.

Regarding morphology, Figure 1 presents the X-ray diffraction plots obtained for P(HB-HV)-casted films and

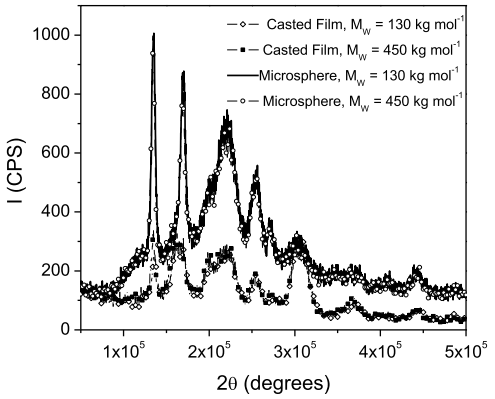

Figure 1. P(HB-HV) X-ray diffraction plots obtained for the casted film of P(HB-HV), M_w = 130 kg mol^{-1} (light diamonds−−straight line); casted film of P(HB-HV), M_w = 450 kg mol^{-1} (dark squares−−straight line); microspheres of P(HB-HV) of M_w = 130 kg mol^{-1} (straight line); and microspheres of P(HB-HV) of M_w = 450 kg mol^{-1} (open circles−−straight line).

microspheres obtained from copolymers with distinct molar masses. It is noteworthy that they are all semicrystalline and that the microspheres present lower degrees of crystallinity than the pure polymer, being 29% for microspheres produced from P(HB-HV) of $\bar{M}_w$ = 450 kg mol^{-1} and 32% for microspheres formed from P(HB-HV) of $\bar{M}_w$ = 130 kg mol^{-1}, whereas films produced with both polymers are 41% crystalline. Figure 2 shows that P(HB-HV) microspheres prepared with the polymers of both molar masses presented a high degree of coalescence and porous surface; moreover, those prepared with P(HB-HV) of $\bar{M}_w$ = 130 kg mol^{-1} presented a broad size distribution (from 30 to 400 μm), whereas those prepared with P(HB-HV) of $\bar{M}_w$ = 450 kg mol^{-1} presented a very narrow size distribution.

To avoid coalescence, distinct contents of the surfactant PVA were added (2.0 and 3.0% w/v), resulting in remarkably reduced average diameters and sharper size distribution for both molar masses with PVA content increase, as evidenced by Figure 3. Larger microspheres with irregular shapes were obtained from P(HB-HV) of $\bar{M}_w$ = 450 kg mol^{-1} and 2.0% w/v PVA, whereas the microspheres resulting from the mixture of higher $\bar{M}_w$ P(HB-HV) with 3.0% w/v PVA were smaller, with narrower size distribution and more uniform shapes.

From Figure 3 it can be observed that the increase of PVA content from 2.0 to 3.0% w/v caused some changes in the average particle diameters or resulted in a sharper size distribution. When the PVA content increase is evaluated in the samples of $\bar{M}_w$(P(HB-HV)) = 130 kg mol^{-1} (images in Figure 3A,E), the particle size distribution became sharper, with the size of particles of 3−8 μm; when using the PVA content of 3% (Figure 3B,F), no particles with diameter higher than 21 μm were observed, whereas in samples containing 2% of PVA, the size distribution is wider and particles of 22−30 μm were found. In samples prepared with $\bar{M}_w$(P(HB-HV)) = 450 kg mol^{-1}, the effect is more pronounced. The size distribution is sharper when the content of PVA is 3% and they

DOI: 10.1021/acsomega.9b00824
ACS Omega 2019, 4, 8122−8135

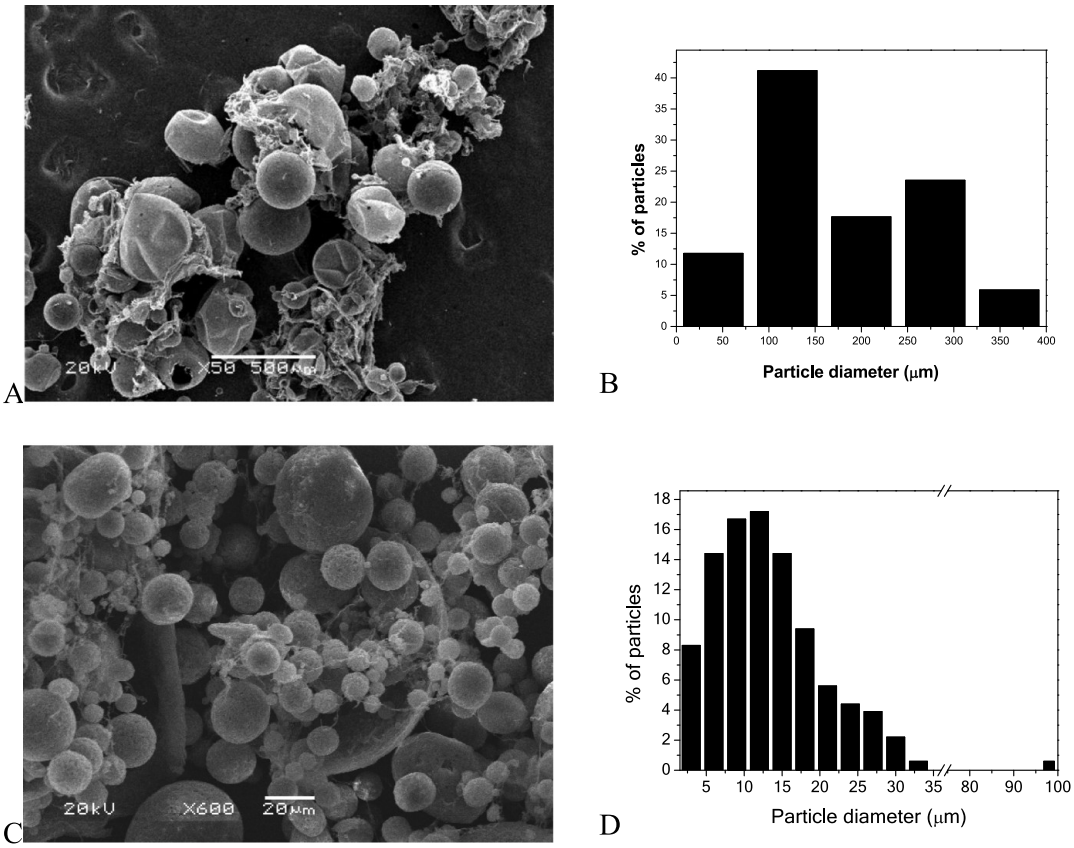

Figure 2. SEM images of 1.0% w/v P(HB-HV) microspheres produced with 1.0% w/v PVA, 300 rpm: (A) $\bar{M}_w$(P(HB-HV)) = 130 kg mol^{-1}and (B) its size distribution; (C) $\bar{M}_w$(P(HB-HV)) = 450 kg mol^{-1} and (D) its size distribution.

presented diameter from >1000 to 11 μm (Figure 3H), whereas samples prepared with 2% of PVA presented diameters in the range of 2−31 μm (Figure 3D). Yet, particle sizes are concentrated in diameters less than 5 μm (Figure 3H) in samples containing 3% of PVA, whereas microspheres of >1000 nm to 2 μm were not found in samples using 2% of PVA, which presented particle sizes concentrated in diameters of 10−15 μm (Figure 3D). Moreover, it affected the shape and homogeneity of the obtained microspheres: when the PVA content is increased to 3.0% w/v, smaller and regular microspheres were obtained.

With respect to the effect of employing distinct encapsulation stirring rate regimes to particle size, in their work, Martin et al.[65] showed that rough and larger PHB microparticles were produced at a low stirring rate regime, whereas at a high stirring rate regime, smaller, but rougher and wrinkled, microparticles were produced. They related this roughness to PHB polymer crystallinity, as, in their samples, even the obtained microparticles presented certain degree of crystallinity. As showed in earlier studies,[66−69] the P(HB-HV) copolymer is semicrystalline and, therefore, it is susceptible to phase separation and its unstable crystals may melt upon heating.[70] Our results, as showed by X-ray diffraction presented in Figure 1, also evidenced some degree of crystallinity of the starting polymer, which led to semicrystalline P(HB-HV) microparticles, when both polymers with distinct molar masses were used in the formulation. Distinct crystallinity, as will be further discussed, influences the microsphere surface characteristics and properties.

The role of encapsulation stirring rates on particle size distribution was evaluated. As shown in Figures 4 and 5, higher stirring rates produced smaller droplets and promoted disruption of larger droplets during solution emulsification, which led to smaller particles of narrow size distribution (Figure 5B,D). Nevertheless, the smallest microparticles (in the range of >1000 nm to 5 μm) were obtained at lower stirring rates. In these conditions, they were produced in an expressive amount, being 15% in samples produced with Py and more than 44% in samples produced with C6 (Figure 4B,D).

The role of the fluorescent dyes (C6 and Py), at a concentration of approximately 200 μg mL^{-1} in formulations, on the particle size and size distribution was studied in protocols using 1.0% w/v P(HB-HV) and 2.0% w/v PVA. As observed by comparing Figures 2A−D to 3E−H, there is a remarkable decrease in size and size distribution when the PVA content is increased from 1.0 to 3.0% w/v, but there is an important size variation when coumarin-6 or pyrene is added to the formulation, as shown in Figures 4 and 5. Microparticles were, initially, smaller upon Py addition, as Figures 3, 5, and 6 show, with nanospheres of 150−180 nm (Figure 6) being formed. Nevertheless, these nanoparticles coalesce to give a wider size distribution than that observed for C6. Although, in these conditions, samples produced with C6 did not present any nanospheres, particles presented smaller sizes, ranging from 2 to 16 μm, presenting more than 30% of particles of 6 μm, whereas for samples prepared with Py as an additive, the size distribution is in the range from 2 to 20 μm, with 25% of particles of 6 μm and 0.5% of particles presenting diameters of

DOI: 10.1021/acsomega.9b00824
ACS Omega 2019, 4, 8122−8135

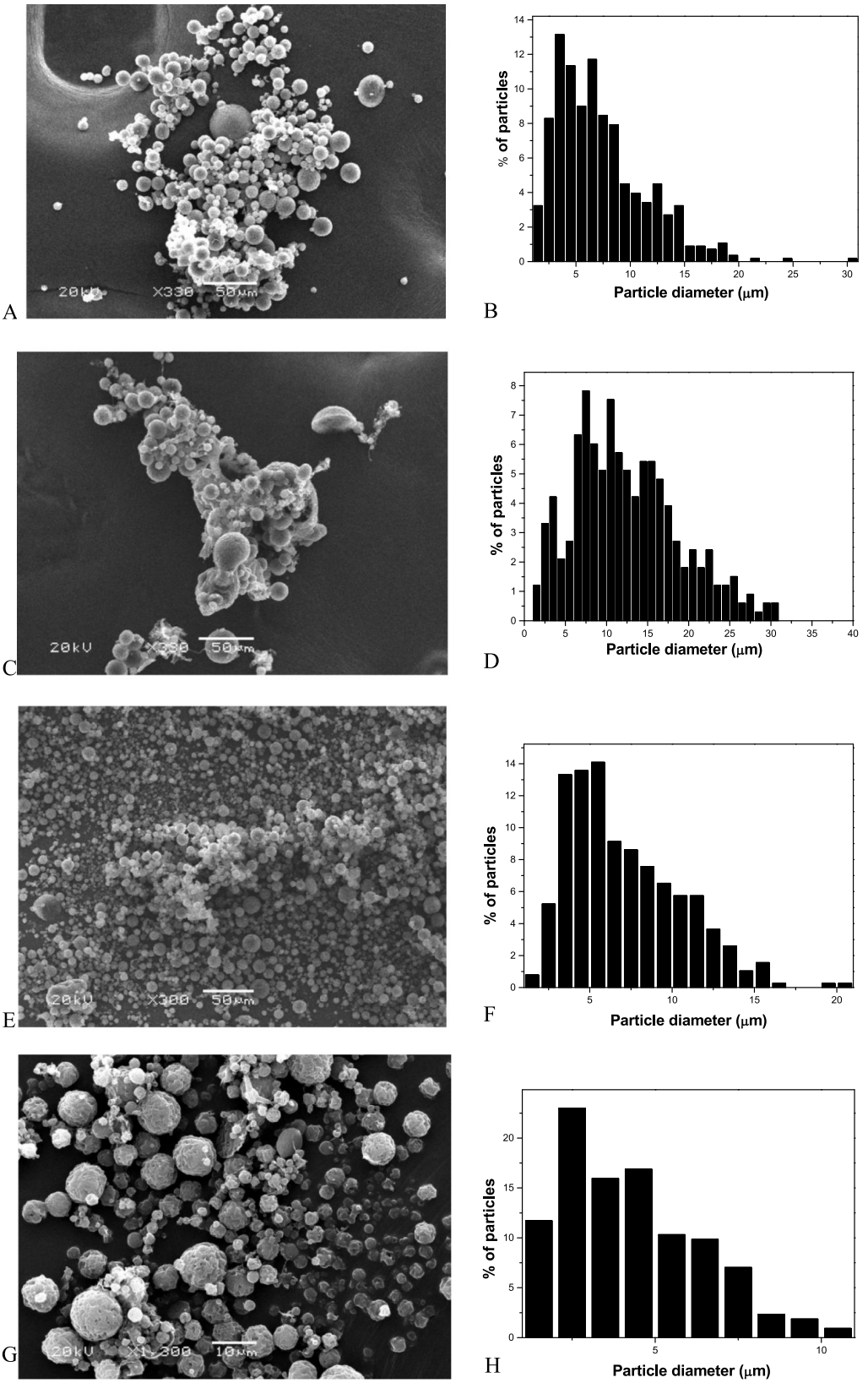

Figure 3. SEM images of 1.0% w/v P(HB-HV) microspheres with 2.0% w/v PVA, 300 rpm: (A) $\bar{M}_w$(P(HB-HV)) = 130 kg mol^{-1} and (B) its size distribution; (C) $\bar{M}_w$(P(HB-HV)) = 450 kg mol^{-1} and (D) its size distribution. Microspheres with 3% w/v PVA, 300 rpm: (E) $\bar{M}_w$(P(HB-HV)) = 130 kg mol^{-1} and (F) its size distribution; (G) $\bar{M}_w$(P(HB-HV)) = 450 kg mol^{-1} and (H) its size distribution.

25 μm (Figure 5D). This is evidence of the average particle size reduction because of the fluorophore-specific interactions with the particle constituents. In fact, as the P(HB-HV) microsphere surface is polar, it may present stronger interactions with C6 than with Py, leading to the observed smaller particles with Py. It is expected that, with the polar C6,

DOI: 10.1021/acsomega.9b00824
ACS Omega 2019, 4, 8122−8135

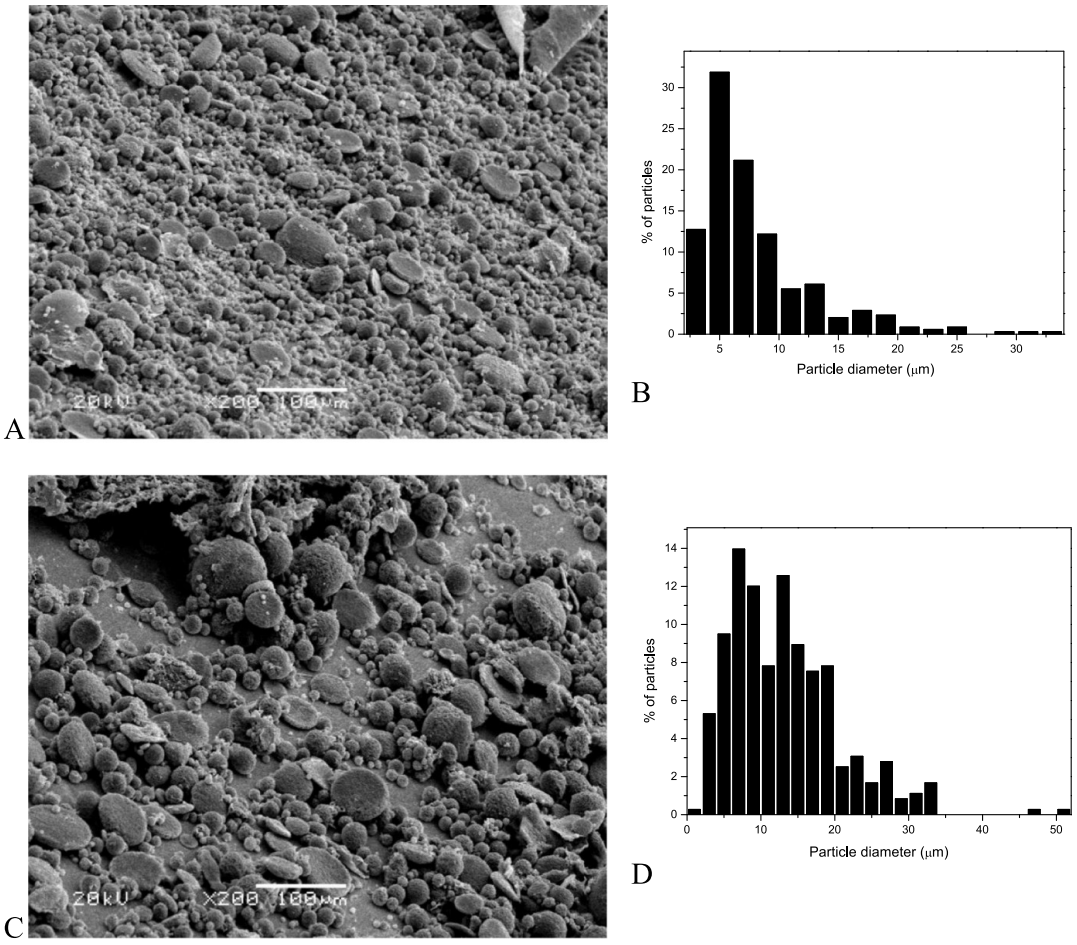

Figure 4. SEM images of 1.0% w/v P(HB-HV) microspheres with 2.0% w/v PVA, $\bar{M}_w$(P(HB-HV)) = 130 kg mol^{-1}: (A) with C6, produced via protocol 2, stirred at 300 rpm (B) and its size distribution; (C) with Py, produced via protocol 5, stirred at 300 rpm and (D) its size distribution. Bars correspond to 100 μm.

P(HB-HV) particles interact specially via electrostatic interactions, which are strong interaction forces, or through Debye forces, as C6 is a permanent dipole. With Py, van der Waals interactions are expected, especially London dispersion forces are also expected, as this compound can present an instantaneous induced dipole in such systems.[71]

As showed by Maia et al.,[10] P(HB-HV) microspheres are also obtained in preparations in the absence of encapsulating compounds. Furthermore, Muramaki et al.[72] showed that highly hydrolyzed PVA, when used as an emulsion stabilizer, led to local gelatinization of the emulsion droplet surfaces and enabled nanoparticle aggregation, resulting in larger particles. In this work, P(HB-HV) nanospheres (150−180 nm) were observed as microspheres' precursors in the presence of Py (Figures 4 and 6). In fact, the emulsion stabilizer PVA used in the solvent evaporation method for microparticle preparation tends to bind to the produced microparticles, affecting some properties of the microsphere, such as its hydrophobicity and degradation parameters, and therefore its erosion rate. Also, the PVA content per weight of the microparticle is expected to change as the particle size decreases because of the specific surface area increase in smaller microparticles.[73−75] PVA binds irreversibly to polymer microparticles, causing a PVA surface density increase as the microparticle size decreases. Nevertheless, this effect is independent of the residual PVA concentration,[73] being virtually the same at the concentration studied (from 0.1 to 10% w/v). In fact, Mu et al.[73] stated that PVA recovers the nanoparticle surface and forms an interconnected network with the polymer at the interface, which hinders its removal after emulsification. This effect herein is referred to as PVA gelatinization.

The effect observed in our work suggests that the nonpolar fluorophore (Py) inhibits surface stabilization by means of repulsion forces. As Py-loaded microspheres are expected to present weaker probe−microsphere−surfactant interaction than those containing C6, the amount of residual PVA is smaller (Table 1). Consequently, surface charge is expected to change and nanometric droplets are formed and initially stabilized, but further aggregation cannot be avoided. Pyrene sorption on the surface of the inner nanometric particles prevented the hydrophilic PVA molecules to coalesce; nevertheless, Py repulsion forces were overcome by hydrophobic forces among P(HB-HV) chains, which enabled droplet aggregation, resulting in nanoparticles coalescence. It suggests that the Py and C6 polarity characteristics changed the surface nanoparticle properties, but in different ways. In fact, nanoparticles based on PHB and its derivatives are only reported in composite preparation.[76−80]

Table 1 also presented the residual PVA contents in all preparations. The reason for the higher PVA residual content when C6 is used, compared to the residual PVA in Py-containing formulations, is related to the nature and magnitude

DOI: 10.1021/acsomega.9b00824
ACS Omega 2019, 4, 8122−8135

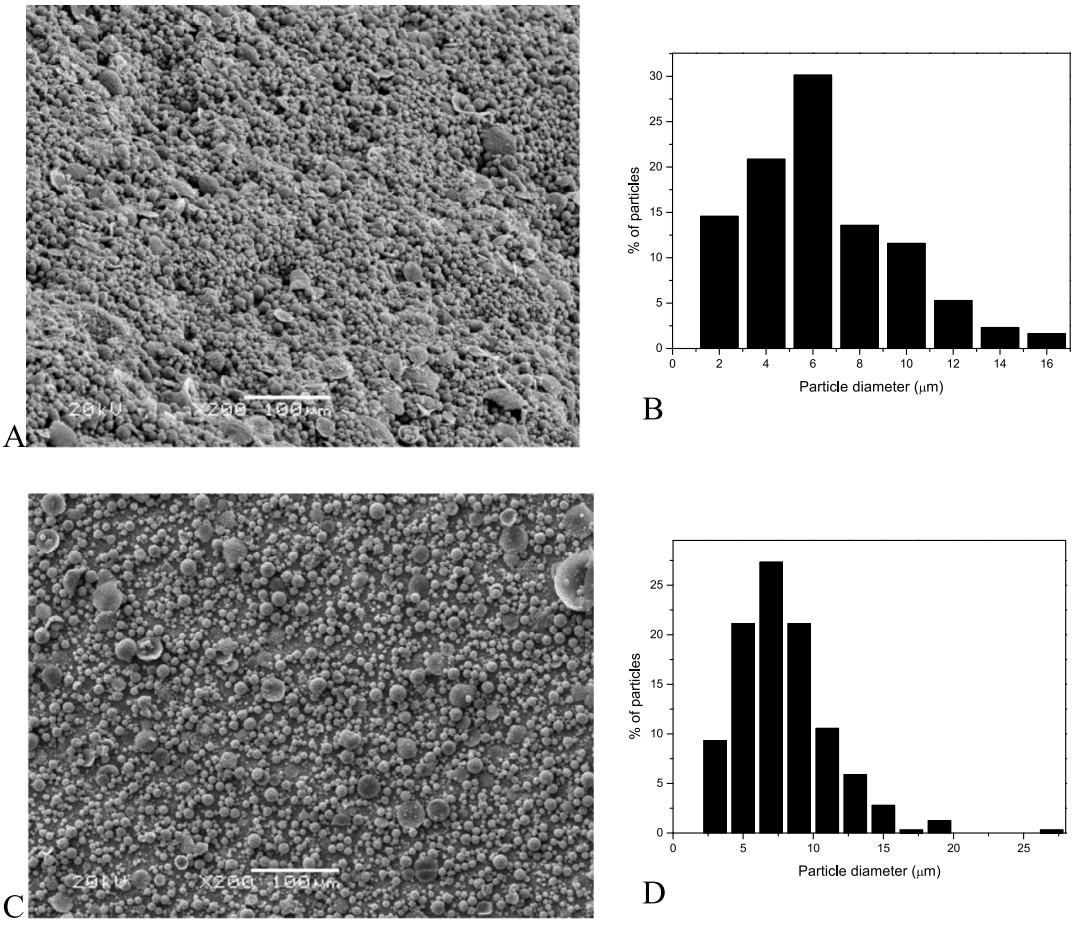

Figure 5. SEM images of 1.0% w/v P(HB-HV) microspheres with 2.0% w/v PVA, $\bar{M}_w$(P(HB-HV)) = 130 kg mol^{-1}: (A) containing C6, produced via protocol 2, stirred at 900 rpm and (B) its size distribution; (C) containing Py, produced via protocol 8, stirred at 900 rpm and (D) its size distribution. Bars correspond to 100 μm.

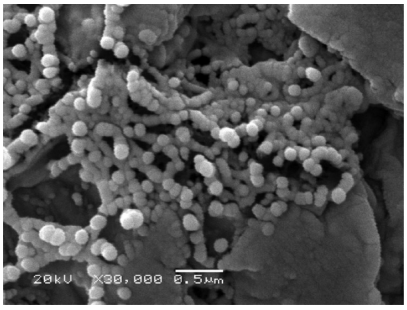

Figure 6. SEM images registered for P(HB-HV) nanospheres at the Py-loaded microsphere surface.

of interactions between the carbonyl groups on C6 lactone and the hydroxyl groups of the residual PVA sorbed on the P(HB-HV) surface. Py does not present such an evident influence on the amount of residual PVA, even when changes in the experimental protocol were implemented, whereas samples containing C6 were sensible to protocol changes and resulted in distinct residual PVA contents, which evidences a remarkable change in surface properties.

The obtained values of ζ-potential presented in Table 1 lead to the conclusion that the greater the probe−polymer interaction, the greater is the PVA deposition and infeasibility of forming nanoparticles (because of the balance of fluorophore nature and polymer hydrophobicity), but higher

Table 1. Microsphere Formulations of 1.0% w/v P(HB-HV), with Particle Size, ζ-Potential, and Residual PVA Results, at 2% w/v PVA and 300 rpm Stirring (Unless Indicated)[a]

protocol	formulation	$\bar{d} \pm \sigma$ (VC, %) (μm)	ζ-potential $\pm \sigma$ (mV)	residual PVA (w/w, %)
1	PVA + P(HB-HV) 130 kg mol^{-1} (formulation 1)	7.4 ± 4.2 (57)	−17.51 ± 0.95	3.5
2	(formulation 1) + C6	9.2 ± 6.7 (73)	−32.85 ± 4.00	9.3
3	(formulation 1) + C6 (900 rpm)	6.4 ± 3.2 (50)	−24.41 ± 3.68	7.1
4	(formulation 1) + C6 + TR	7.6 ± 5.1 (67)	−21.95 ± 3.30	5.1
5	(formulation 1) + Py	18 ± 8 (70)	−10.53 ± 1.44	4.7
6	(formulation 1) + Py (900 rpm)	7.8 ± 3.3 (43)	−12.83 ± 1.09	4.8
7	(formulation 1) + Py + TR	21 ± 8.0 (60)	−6.91 ± 1.44	4.8

[a]TR = trehalose.

DOI: 10.1021/acsomega.9b00824
ACS Omega 2019, 4, 8122−8135

particle stabilization levels were reached, smaller microparticles were obtained, and the surface charge was enhanced. However, dipolar and hydrogen-bonding interactions between the carbonyl and amino groups of C6 and the carbonyl groups of P(HB-HV) are more effective than the induced dipole−dipole interactions between P(HB-HV) and Py. Once again, the fluorophore characteristics were determinants in the microsphere formation, evidenced by the capture and encapsulation efficiencies. The decrease of the total surface charge because of weaker hydrophobic interactions between the copolymer and Py facilitates interparticle attraction and surface adherence, enabling the nanospheres to coalesce and give rise to large sphere-like particles.

2.2. Microsphere Surface Properties. From the SEM images presented in Figures 3−5, it is evident that surface roughness is modulated by the additive contents and chain lengths of P(HB-HV) copolymers. From these images, longer P(HB-HV) chains lead to rougher surfaces, fluorophore-containing microspheres are smoother than the microspheres without fluorophores, and those formed upon protocols with less PVA content are rougher than those formed upon higher PVA contents in the formulation. To infer on the particle surface morphology and the reasons of such diversity, chemical analyses of the residual PVA and C6 or Py sorbed on the particles' surface were performed. PVA polymeric chains present a hydrophilic portion with a higher volume than the hydrophobic portion; therefore, it is expected that they would be able to form very stable oil/water emulsions, as micelles are formed. It leads to the assumption of a denser coverage of the hydrophobic portion of several PVA molecules, forming droplets with increased superficial density until reaching the point of saturation, at the size limit of the drops, which generates a residual content of the surfactant.[73,81] Partially hydrolyzed PVA (around 70%) presents more hydrophilic portions than a highly hydrolyzed one, such that used in this work. Nevertheless, at lower degrees of hydrolysis, the polymer solubility is highly affected, limiting its use as a stabilizer. Along with the superficial density, the so-called "blockiness"[82−84] of the PVA hydrophobic portion influences its emulsifying ability. Although partially hydrolyzed PVAs are excellent stabilizers for aqueous and flat systems, PVAs with higher degrees of hydrolysis are very efficient to stabilize oil/water emulsions,[76] such that employed here and also by Tian et al.[85] This surfactant residue can be determined by UV/vis absorption, once it can form complexes with in situ generated iodine and the absorbance variation is measured at 690 nm; the complexes are with the maximum absorption wavelength. It was found that the residual PVA content depends on the presence of the fluorophores. In these terms, the residual PVA content in the control sample of 2.0% w/v PVA + 1.0% w/v P(HB-HV) 130 kg mol^{-1} was 3.5%. Table 1 shows the residual PVA contents of all samples. C6-containing microspheres showed the highest residual PVA content of 9.3% w/w, on average, which is almost twice the content found for Py-containing microspheres (4.7% w/w, on average). In addition, the ζ-potential data showed that particle surfaces containing C6 are more negative than the particles with no fluorophore added, and those containing Py are the less negative particles. Data are shown in Table 1.

Microspheres obtained in this work presented rougher surface and smaller structures as the encapsulation stirring rate is increased. Nevertheless, our findings show that the surfactant content is a determinant to microsphere size control and plays an important role in the surface roughness. This was also found by Maia et al.[10] In addition, Panith et al.[11] showed that an increase in the HV content in the P(HB-HV) polymer leads to more spherical particles with smoother and less porous surface morphology. This is attributed to the lower crystallinity of the copolymer compared to the PHB homopolymer microspheres. In this work, the HV % is very low, being higher in P(HB-HV) of M_w = 130 kg mol^{-1}, which is 2.7% for this copolymer, and yet it seems to influence the dispersion of the organic phase in the aqueous media, acting as a surfactant, as mentioned before. From Figure 3, on the other hand, P(HB-HV) of M_w = 450 kg mol^{-1}, with less HV % (0.7%), produced a highly rough and porous surface, which evidenced the effect as being due to the polymer chain lengths than due to HV %, at such low contents.

The surfactant PVA also acted as a cryoprotector during the lyophilization process in the substitution of trehalose and as an agglutination preventive, as it prevents the freeze-drying powdered microsphere aggregation, which is expected to occur with no trehalose addition to the mixture.[86] Initially, the sample is immersed in $N_{2(liquid)}$, at 77 K, to eliminate water in excess through sublimation of the small ice crystals formed at this step. Then, the maximum drying temperature must be kept below the microsphere glass transition temperature (T_g) to avoid fusion and agglutination. As PVA T_g (approx. 350 K) is higher than P(HB-HV) T_g (approx. 273 K), during lyophilization at 283 K, the surfactant remained in its glassy state, whereas the P(HB-HV) microspheres became fluid, which maintained the particles apart and stable, avoiding aggregation. After redispersion, the particles showed the same physical characteristics with and without trehalose,[87] which showed that trehalose is dispensable to the proposed formulations.

2.3. C6 and Py Encapsulation Efficiencies. The lyophilized microspheres were analyzed with respect to three encapsulation aspects: (1) recovered percentage (% rec) upon lyophilization, (2) fluorophore capture efficiency (% ads), and (3) fluorophore encapsulation efficiency (% EE). They were determined by eqs 1−3, described in the Experimental Section. The calculated efficiencies are presented in Table 2.

Table 2. Microsphere Properties of 1.0% w/v P(HB-HV) 130 kg mol^{-1} + 2.0% w/v PVA with C6 and Py: Recovered Percentage, % rec (Eq 1), Fluorophore Capture Efficiency, % ads (Eq 2), Fluorophore Encapsulation Efficiency, % EE (Eq 3)

sample	formulations	% rec	% ads	% EE
2	+C6 (300 rpm)	61	14	96
3	+C6 (900 rpm)	54	14	98
4	+C6 + trehalose (300 rpm)	65	8	100
5	+Py (300 rpm)	48	2	15
6	+Py (900 rpm)	52	3	19
7	+Py + trehalose (300 rpm)	57	2	17

As Py weakly interacts with PVA and P(HB-HV) polymers, microspheres produced in the presence of this fluorophore are expected to present a reduced capture efficiency and, indeed, it was four to eight times less effective than the capture efficiency determined for samples containing C6 (Table 2), even though P(HB-HV) conversion into microspheres, in the presence of any of these fluorophores, occurred at the same proportion (approximately 60%, see Table 2).

2.4. Fluorescence Confocal Laser Microscopy. Figures 7 and 8 present fluorescence confocal laser micrographs

DOI: 10.1021/acsomega.9b00824
ACS Omega 2019, 4, 8122−8135

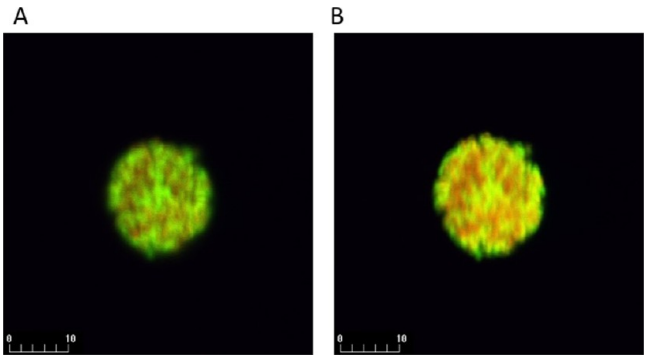

Figure 7. FCLSM images of P(HB-HV) microspheres containing C6. (A) At the surface section of a selected microsphere and (B) at its center section. Inner scales are micrometers.

registered for microspheres containing C6 or Py. They show distinct fluorescent regions along the equatorial exploitation of the samples, which evidenced the presence of C6 and Py inside the microspheres, as expected, because of fluorophore encapsulation. Notably, fluorophores are distinctly distributed in the copolymer matrix.

Figure 7 shows equatorially cut micrographs of C6-containing microspheres at the center section and at the surface of the microsphere. Distinct colors are due to the distinct moieties emitting at the surface and at the interior of the particles. Image in Figure 7A shows fluorescence predominantly green, which corresponds to emission at the range of 522−535 nm (fluorescence spectra were not shown), which are due to the presence of C6 monomers preferably located at the outermost layers of the microsphere. Figure 7B, however, presents a predominantly yellow-red fluorescence, at the range of 580−632 nm, which is due to the C6 aggregates located at the inner section of the microsphere. The red-shift effect of the fluorescence spectra occurs when fluorophores interact to emit from the relaxed excited states, and this is the effect frequently caused by aggregation. This aggregation occurs more efficiently in the interior of the microsphere because the fluorophore moieties are closer to each other, resulting in effective interactions and revealing that a considerable amount of fluorophore was encapsulated.

In Figure 8, Py-containing microspheres showed a distinct distribution compared to the C6-containing ones. Figure 8A presents a microsphere with fluorescence predominantly green, which indicates greater amounts of Py in the regions closer to the surface as aggregates (excimer fluorescence in the green region, between 522 and 535 nm; fluorescence spectra not shown). From Figure 8B, which corresponds to the image taken from the equatorial section at the center of the microsphere, it is possible to observe "dark" sites inside the microsphere, attributed to the absence of fluorophore or to the fluorescence typically emitted by the monomers of Py, at the UV region, between 372 and 394 nm (similar to the spectra shown in Figure 11).

2.5. Controlled Release Kinetics. By steady-state fluorescence spectroscopy, the kinetics of fluorophore release from the microspheres were determined. In Figure 9 are presented fluorescence spectra recorded for microspheres produced via protocols 2 and 3, that is, containing C6, as a function of time. The spectral characteristics of C6 are obtained, and it is observed that their intensity increase with time.

Fluorescence intensity of C6 over time was used to determine the concentration of free C6 ($[C6]_{free}$) in the solution (Figure 10A), which informs about the release rate. $[C6]_{free}$ is lower in microspheres produced via protocol 2 (Table 1) and, to avoid deviations, the release rate is determined in a plot of percentage of released C6 (% C6) over time, which is presented in Figure 10B.

Steady-state fluorescence spectra recorded for microspheres containing pyrene, prepared via distinct protocols (5 and 6, Table 1), are presented in Figure 11. They show the characteristic fluorescence of pyrene, and there is no evidence of excimers or dimers in these samples.

As pyrene is well-known as a polarity-sensitive compound, the intensity ratio of vibronic peaks in the fluorescence spectra at 374 nm and at 394 nm (I_{374}/I_{394}) was determined over time, for both preparations. The results are presented in Table S2 in the Supporting Information.

The intensity change of fluorescence over time was also used to determine the concentration of pyrene that is released ($[Py]_{free}$), and the plots of $[Py]_{free}$ versus time and percentage of pyrene (% Py) released over time are presented in Figure 10C,D.

This above-mentioned polarity sensitivity of pyrene is characterized by changes in the fluorescence spectra, and it

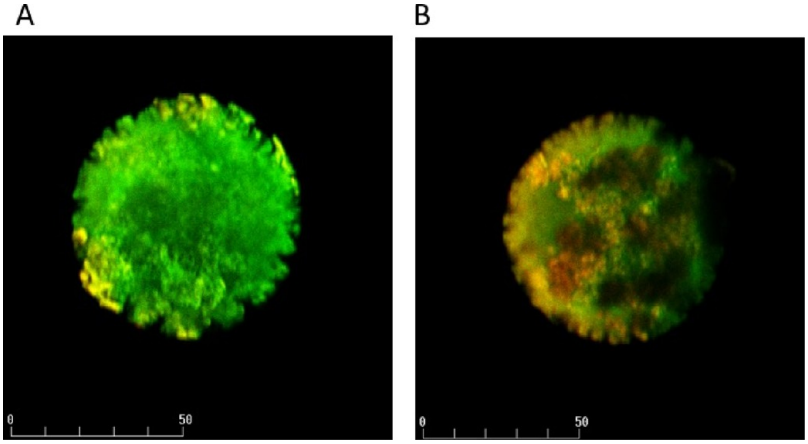

Figure 8. FCLSM images of P(HB-HV) microspheres containing Py. (A) At the surface section of a selected microsphere and (B) at its center section. Inner scales are micrometers.

DOI: 10.1021/acsomega.9b00824
ACS Omega 2019, 4, 8122−8135

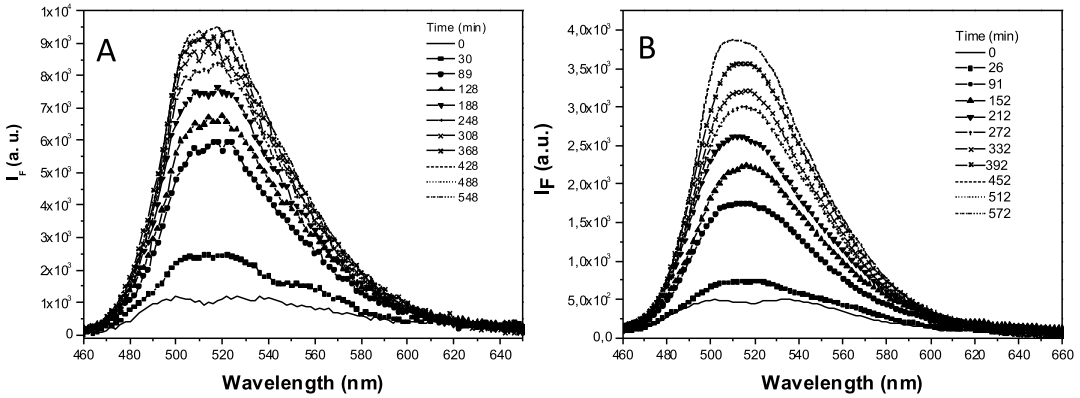

Figure 9. Steady-state fluorescence spectra recorded for microspheres containing C6, formed with 2% m/v of PVA + 1% m/v of P(HB-HV) + coumarin-6: (A) 300 rpm, seven washing cycles and (B) 900 rpm, seven washing cycles.

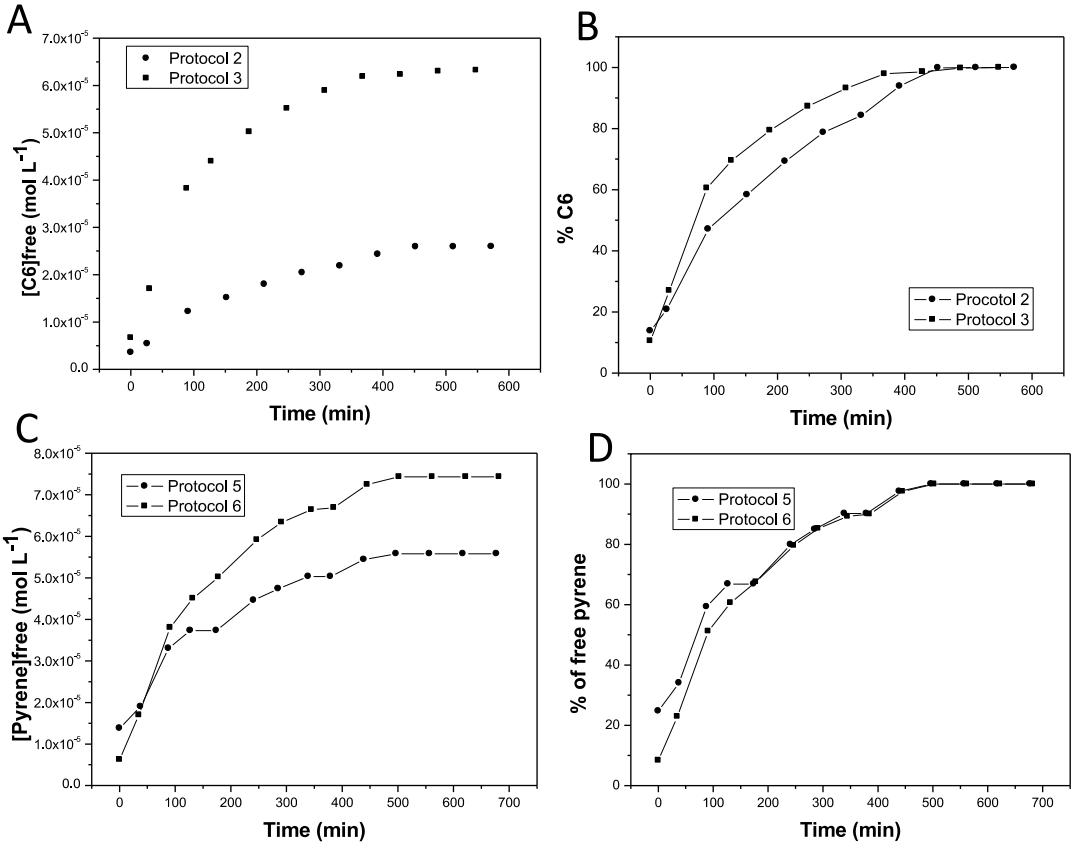

Figure 10. Curves of (A) $[C6]_{free}$ vs time; (B) % of free C6 vs time for microspheres produced via protocols 2 (●) and 3 (■); (C) $[Py]_{free}$ vs time and (D) % of free Py vs time for microspheres produced via protocols 5 (●) and 6 (■).

is due to the self-absorption effect that is stronger in nonpolar environments, leading to a reduced relative intensity of fluorescence peaks (I_{374}/I_{394}). By analyzing I_{374}/I_{394} values, obtained for the pyrene fluorescence spectra recorded at distinct times, during the controlled release determination, from the microspheres produced by both protocols 5 and 6, it is evident that pyrene is in a polar environment in both samples; nevertheless, it shows that the local polarity of microspheres produced via protocol 6 is slightly higher than that of the microspheres produced via protocol 5. It can be related to an effect of the PVA moieties, which are hydrophilic and maybe distinctly spread over microspheres produced at stirring rates imposed to each protocol. Also, as showed by Sahoo et al.,[88] it can form a hydrogel over the microspheres, generating a diffusional barrier to the release of both pyrene and coumarin-6, which could lead to a distinct release of fluorophores in microspheres produced by the adopted stirring rates. In fact, for an oil-in-water emulsion, Py is the dominant component in lowering surface tension in the initial nanoparticles and, therefore, accumulates at the oil−water interface.[89]

Regarding the controlled release kinetics of fluorophores, Figure 10 showed that samples produced with both fluorophores, in both stirring conditions, present a fast initial release phase, with a release of approximately 60% of the fluorophores at the first 100 min. This effect is independent of the identity of the fluorophore, but it is faster for those samples that resulted in microspheres of smaller size distributions, such

DOI: 10.1021/acsomega.9b00824
ACS Omega 2019, 4, 8122−8135

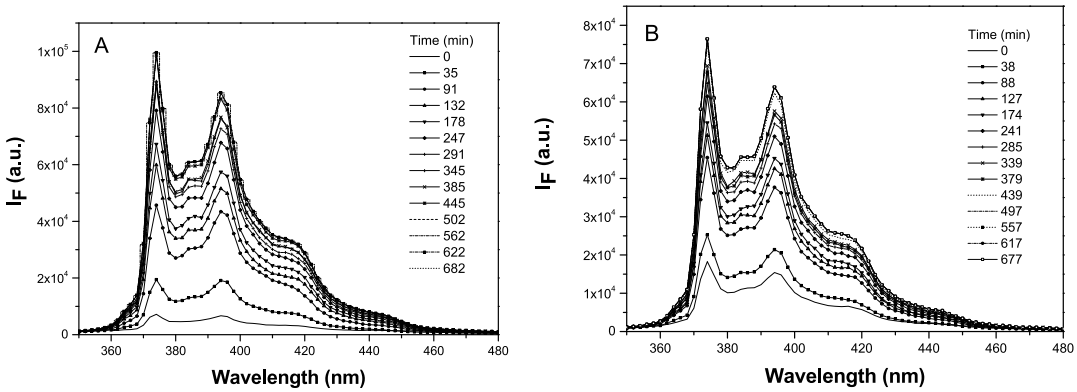

Figure 11. Steady-state fluorescence spectra recorded for microspheres containing Py, formed with 2% m/v of PVA + 1% m/v of P(HB-HV) + pyrene: (A) 300 rpm, seven washing cycles and (B) 900 rpm, seven washing cycles.

as those prepared via protocols 3 and 6 (Table 1). This may be because of a higher superficial area in these samples and of the release of fluorophores that are not in the interior of the microspheres. Nevertheless, from 100 min, there are differences in the release rates. Samples containing pyrene present virtually the same release kinetics, whereas for samples containing C6, the release from the smaller microspheres (those prepared via protocol 3) is faster than the release from larger microspheres. This distinct behavior between the microspheres of Py and C6 may be because of the differences in polarity of these fluorophores and, thus, of the distinct interaction nature between the fluorophore and polymeric matrices. As pyrene is a nonpolar compound, it weakly interacts with the polymeric chains, whereas C6 interacts with them by strong electrostatic interactions and hydrogen bonds. In all cases, all encapsulated fluorophores are released at times of approximately 450 min; the initial release occurred by diffusional mechanisms, followed by an erosion of the microspheres that lad to the fluorophore release.

3. CONCLUSIONS

In this work, we showed that, although the use of fluorophores in the P(PH-HV) microsphere production does not significantly influence their morphological characteristics, fluorophore characteristics presented a role in particle properties assignment, including size, size distribution, surface charge, and entrapment efficiency. By comparing the microspheres produced under distinct conditions, such as polymer molar mass, stirring rates, and surfactant and fluorophore contents, it was clear that the P(HB-HV) molar mass exerted a high influence on the size and surface morphology. Fluorophore capture and fluorophore encapsulation efficiencies were modulated by the interaction balance between P(HB-HV) and fluorophores, showing stronger effects in C6-containing microspheres than in Py-containing ones.

The final sizes of microspheres are driven by the PVA concentration because of its ability to avoid coalescence of the droplets formed during stirring. As nanospheres were observed in this work, in samples produced with the fluorophore Py, and as they are expected to give rise to microspheres, it is evidences that PVA gelatinization onto nanosphere surfaces influenced the balance between the aggregation forces of polymeric chains and the repulsion forces exerted by the Py molecules. It evidences that the nonpolar Py avoids gelatinization in the first-obtained nanoparticles by repulsion forces, but, at some point, polymeric aggregation is strong enough to enable microsphere formation. C6-specific interactions with P(HB-HV) and PVA moieties are stronger than those with Py and contribute to gelatinization in first cores, inhibiting nanoparticle formation. Also, residual PVA in the particle surface avoided the aggregation of the microparticles. Such results showed that trehalose was dispensable in the formulation as a cryoprotector during lyophilization, and PVA acts also as an efficient cryoprotector.

By FCLSM, it was shown that C6 is distributed throughout the inner core of the microparticle, whereas Py was concentrated at its surface.

The controlled release kinetics of both fluorophores presented a similar initial phase driven by diffusion, which is independent of fluorophore identity, but determined by the microsphere size distribution. Further release phases are strictly dependent on the fluorophore properties and the nature of their interaction with the P(HB-HV) and PVA moieties, which are highly hydrophilic and can distinctly influence the diffusion of C6 and Py. Nevertheless, the total release of both fluorophores was reached at a similar time, of approximately 450 min.

4. EXPERIMENTAL SECTION

4.1. Microsphere Preparation. Poly(hydroxybutyrate-*co*-hydroxyvalerate) [P(HB-HV)] $\bar{M}_w$ = 130 kg mol^{-1} (96.9% PHB/2.70% PHV) and 450 kg mol^{-1} (98.8% PHB/0.70% PHV) were purchased from Usina da Pedra—Irmãos Biagi S.A. (Brazil). PVA ($\bar{M}_w$ = 124−186 kg mol^{-1}, 98−99% hydrolyzed) was supplied by Sigma-Aldrich. Chloroform P.A. was purchased from Tedia (Brazil) and was previously purified. Coumarin-6 (C6) 99% and pyrene (Py) 99% were supplied by Sigma-Aldrich. Their chemical structures are shown in the Supporting Information (Figure S1).

Microspheres containing fluorophores C6 or Py and microspheres without fluorophores were prepared by distinct protocols that used distinct quantities of P(HB-HV) copolymer, PVA, in the presence and absence of trehalose. They consisted of the dissolution of an amount (1.0% w/v) of the P(HB-HV) copolymer in a 0.1% w/v C6 or Py chloroform solution, at room temperature (298 K). A 30 mL of this resulting solution was added to 120 mL of 1.0, 2.0, or 3.0% w/v PVA aqueous solution. The obtained emulsion was homogenized by mechanical stirring at 300 rpm or 900 rpm, continuously, for 24 h, in an open flask to enable solvent evaporation. The microspheres were then centrifuged in a Beckman centrifuge J2-21 at 10 000 rpm and washed twice

DOI: 10.1021/acsomega.9b00824
ACS Omega 2019, 4, 8122−8135

with deionized water, freeze-dried in a Thermo Savant MicroModulyo-115 lyophilizer, and stored in vacuum desiccators at room temperature (298 K). Other protocols consisted of the addition of 180 mg of trehalose as a cryoprotector after emulsion preparation, in the proportion of 0.12% w/v.

The amounts of C6 and Py incorporated in the microspheres were determined by UV/vis absorption spectroscopy in a HP 8453 diode array spectrophotometer. For this determination, the fluorescent molecules were desorbed from the microspheres, powdering 5 mg of the produced microspheres, and dispersing this powder in 10 mL of chloroform under stirring for 20 min to dissolve the polymer and to extract the fluorophore. A 200 μL of this supernatant containing C6 or Py was diluted in 2.5 mL of purified chloroform. Its concentration was determined by applying the obtained absorbance data to a calibration curve constructed in the fluorophore concentration range from 1.0×10^{-5} to 1.0×10^{-6} mol L^{-1}, at wavelengths of 446 and 338 nm, which are the maximum absorption wavelengths for C6 and Py, respectively. On the basis of these data, the recovered percentage (% rec), the fluorophore capture efficiency (% ads), and the fluorophore encapsulation efficiency (% EE)[90] were calculated, as follows

$$\%\ \text{rec} = \frac{m_l}{m_p + m_f} \times 100 \quad (1)$$

$$\%\ \text{ads} = \frac{m_{f,l}}{m_{f,l} + m_l} \times 100 \quad (2)$$

$$\%\ \text{EE} = \frac{C_{C6,Py} V_i}{m_m} \left[\frac{(m_f + m_p + m_{PVA,Tls})}{m_f} \right] \times 100 \quad (3)$$

where $C_{C6,Py}$ is the C6 or Py concentration in chloroform after microsphere extraction; V_i is the chloroform volume used in microsphere dissolution; m_l is the lyophilized microsphere mass; m_p is the initial polymer mass; m_f is the fluorophore mass; $m_{f,l}$ is the fluorophore mass into lyophilized microspheres; m_m is the microsphere mass used in the analysis; m_f is the C6 or Py mass, m_p is the P(HB-HV) mass, $m_{PVA,Tls}$ is the PVA or trehalose mass used in the microsphere preparation.

Because of the experimental evidence that smaller particles with sharper size distribution are obtained when using the PVA content of 2.0% w/v in microspheres without fluorophores or containing fluorophores, this PVA concentration was selected to be employed at all further protocols of formulations. These variables of composition were elected according to $a2^5$ degrees of freedom factorial planning of the experiments, as summarized in Table S1. The variables of the adopted procedure were the presence or absence of a fluorophore (C6 or Py), which is variable 1, the presence represented by a (+) signal and absence by a (−) signal; variable 2 being P(HB-HV) of $\bar{M}_w$ = 130 kg mol^{-1}, represented by a (−) signal or P(HB-HV) $\bar{M}_w$ = 450 kg mol^{-1}, represented by a (+) signal; variable 3 being the double quantity of PVA, represented by (−) or triple quantity of PVA, represented by (+); variable 4 being the presence (+) or absence (−) of trehalose as a cryoprotector; and variable 5 being the stirring rate with 300 rpm represented by (−) signal and 900 rpm represented by (+). It is noteworthy that, as two distinct fluorophores were used in these protocols, the total number of experiments performed for procedure optimization was 48. They were performed as indicated in Table S1. The quantity of PVA was varied because the PVA used was 98−99% hydrolyzed, which is a highly hydrolyzed emulsifier and its effect on the P(HB-HV) particle formation should be characterized.

The results for all the samples produced according to Table S1 were compared to those obtained by the procedure employing 1% of PVA content to understand the benefits of changing the PVA content as well as the effects of using a fluorophore to monitor the particles formed and to be encapsulated as models for drugs with distinct hydrophilicity.

4.2. Particle Characterization. The morphologies and physical−chemical properties of the obtained microspheres were characterized, and the experimental details are presented as follows.

4.2.1. SEM Images. The morphology and particle size distribution of lyophilized microspheres were examined by a JEOL JSM-6360-LV scanning electron microscope, operating in the secondary electron image mode with an accelerated voltage of 5 keV. The microspheres were placed in a copper sample holder and metallization was carried out in a Bal-Tec MED 020 sputtering chamber. Magnifications are presented in the respective images.

The diameter of the dried particles was SEM image-analyzed, employing Image Tool 3.0 software,[91] counting 350−600 particles per image. The dimensions of each microsphere were evaluated after a calibration, and each value was statistically treated, determining the average diameter ($\bar{d}$), the standard deviation (σ), and variation coefficient (VC, %). A system is considered monodisperse if VC is less than 10%. Data are presented in Table 1.

4.2.2. Zeta Potentials. The ζ-potentials of the microspheres were determined by electrophoresis of the deionized water suspended particles, after sonication for 5 min, using a ZetaPals Brookhaven, Inst. Corp. apparatus. An acrylic cell was used and inserted with its integral gold electrodes close to the lid.

4.2.3. PVA Residual Content Determination. Microsphere residual PVA contents were determined by the UV/vis absorbance spectra of their complexes with iodine moieties. Complex formation between the alcohol end groups of hydrolyzed PVA and iodine was performed by treating 2 mg of microspheres with 2 mL of 2 mol L^{-1} aqueous NaOH solution for 30 min, at 373 K. Then, the sample was neutralized by adding 1 mL of 4 mol L^{-1} aqueous HCl solution. Then, 3 mL of 0.65 mol L^{-1} boric acid, 1.5 mL of deionized water, and 0.5 mL of I_2/KI (0.05 mol L^{-1}/0.15 mol L^{-1}) were added to the solutions. The absorbance of each sample was measured at λ = 690 nm after 15 min incubation in the dark. The residual PVA contents were determined in a calibration curve of PVA submitted to the same reaction conditions.[92]

4.2.4. FCLSM Images. FCLSM was performed using a Karl Zeiss inverted microscope model MRC 1024 UV, equipped with an argon−krypton laser, an acquisition and analysis system, and a Focus Graphics photographic system. Resuspended microspheres in deionized water were excited at 476, 488, 568, and 647 nm.

4.3. Fluorophore Controlled Release Kinetics. The controlled release kinetics of coumarin-6 (C6) and pyrene (Py) encapsulated in microspheres produced by protocols 2, 3, 5, and 6 (see Table 1) were determined by steady-state fluorescence spectroscopy in an ISS-PC1 spectrophotometer. The samples were placed in a 1 cm optical path quartz cuvette. Microspheres were suspended in a phosphate buffer at pH = 7.4 and Pluronic F-65% m/v, at 310 K, with the spectra recorded at intervals of 30 min for 12 h.

DOI: 10.1021/acsomega.9b00824
ACS Omega 2019, 4, 8122−8135

■ ASSOCIATED CONTENT

Supporting Information

The Supporting Information is available free of charge on the ACS Publications website at DOI: 10.1021/acsomega.9b00824.

Chemical structures of coumarin-6 (C6), pyrene (Py), and PHB and its copolymer poly(hydroxybutyrate-*co*-hydroxyvalerate) [P(HB-HV)]; factorial planning 2^5 of microsphere preparation, considering two distinct fluorophores; and I_{374}/I_{394} ratio determined for the microspheres prepared with 2% m/v of PVA + 1% m/v of P(HB-HV) + pyrene: 300 rpm, seven washing cycles and 900 rpm, seven washing cycles (PDF)

■ AUTHOR INFORMATION

Corresponding Author

*E-mail: tatiana@ufg.br.

ORCID

Tatiana Duque Martins: 0000-0003-1209-9143

Present Address

[§]Triplete Alianca Publicidade e Comunicacao EIRELI-ME. 86.062-600, Londrina, Brazil.

Notes

The authors declare no competing financial interest.

■ ACKNOWLEDGMENTS

This work was supported by FAPESP and CNPq. The authors acknowledge these agencies and CAPES for scholarships. The authors also thank Prof. Teresa Atvars for relevant discussions.

■ REFERENCES

(1) Kojima, R.; Yoshida, T.; Tasaki, H.; Umejima, H.; Maeda, M.; Higashi, Y.; Watanabe, S. Release mechanisms of tacrolimus-loaded PLGA and PLA microspheres and immunosuppressive effects of the microspheres in a rat heart transplantation model. *Int. J. Pharm.* **2015**, *492*, 20−27.

(2) Mo, G.-Z.; Wu, Y.-C.; Hao, Z.-F.; Luo, Q.-F.; Liang, X.-Y.; Guan, L.-T.; Wang, Z.-Y. Synthesis and characterization of a novel drug-loaded polymer, poly(lactic acid-co-aminomethyl benzimidazole). *Des. Monomers Polym.* **2015**, *18*, 536−544.

(3) Andrés-Guerrero, V.; Zong, M.; Ramsay, E.; Rojas, B.; Sarkhel, S.; Gallego, B.; de Hoz, R.; Ramírez, A. I.; Salazar, J. J.; Triviño, A.; Ramírez, J. M.; del Amo, E. M.; Cameron, N.; de-las-Heras, B.; Urtti, A.; Mihov, G.; Dias, A.; Herrero-Vanrell, R. Novel biodegradable polyesteramide microspheres for controlled drug delivery in Ophthalmology. *J. Controlled Release* **2015**, *211*, 105−117.

(4) Prajapati, V. D.; Jani, G. K.; Kapadia, J. R. Current knowledge on biodegradable microspheres in drug delivery. *Expert Opin. Drug Delivery* **2015**, *12*, 1283−1299.

(5) Martins, I. M.; Barreiro, M. F.; Coelho, M.; Rodrigues, A. E. Microencapsulation of essential oils with biodegradable polymeric carriers for cosmetic applications. *Chem. Eng. J.* **2014**, *245*, 191−200.

(6) Fernandes, B.; Silva, R.; Ribeiro, A.; Matamá, T.; Gomes, A. C.; Cavaco-Paulo, A. M. Improved Poly (D,L-lactide) nanoparticles-based formulation for hair follicle targeting. *Int. J. Cosmet. Sci.* **2015**, *37*, 282−290.

(7) Carbone-Howell, A. L.; Ouimet, M. A.; Uhrich, K. E. Biodegradable, bioactive-based poly(anhydride-esters) for personal care and cosmetic applications. In *Polymers for Personal Care and Cosmetics*; Patil, A., Ferritto, M. S., Eds.; ACS Symposium Series; Oxford University Press, 2013; Vol. *1148*, Chapter 9, pp 145−155.

(8) Capan, Y.; Jiang, G.; Giovagnoli, S.; Na, K.-H.; DeLuca, P. P. Preparation and characterization of poly(D,L-lactide-co-glycolide) microspheres for controlled release of human growth hormone. *AAPS PharmSciTech* **2003**, *4*, 147−156.

(9) Hanson, G.; Hanson, B. Fluorescent probes for cellular assays. *Comb. Chem. High Throughput Screening* **2008**, *11*, 505−513.

(10) Maia, J. L.; Santana, M. H. A.; Ré, M. I. The effect of some processing conditions on the characteristics of biodegradable microspheres obtained by an emulsion solvent evaporation process. *Braz. J. Chem. Eng.* **2004**, *21*, 01−12.

(11) Panith, N.; Assavanig, A.; Lertsiri, S.; Bergkvist, M.; Surarit, R.; Niamsiri, N. Development of tunable biodegradable polyhydroxyalkanoates microspheres for controlled delivery of tetracycline for treating periodontal disease. *J. Appl. Sci.* **2016**, *133*, 44128.

(12) Wei, D.-X.; Dao, J.-W.; Liu, H.-W.; Chen, G.-Q. Suspended polyhydroxyalkanoate microspheres as 3D carriers for mammalian cell growth. *Artif. Cells, Nanomed., Biotechnol.* **2018**, *46*, 473−483.

(13) Jan, S.; Roblot, C.; Courtois, J.; Courtois, B.; Barbotin, J. N.; Séguin, J. P. 1H NMR spectroscopic determination of poly 3-hydroxybutyrate extracted from microbial biomass. *Enzyme Microb. Technol.* **1996**, *18*, 195−201.

(14) Deng, X. M.; Hao, J. Y. Synthesis and characterization of poly(3-hydroxybutyrate) macromer of bacterial origin. *Eur. Polym. J.* **2001**, *37*, 211−214.

(15) Mosejko-Ciesielska, J.; Kiewisz, R. Bacterial polyhydroxyalkanoates: Still fabulous? *Microbiol. Res.* **2016**, *192*, 271−282.

(16) Peptu, C.; Kowalczuk, M. Biomass-derived polyhydroxyalkanoates: biomedical applications. In *Biomass as Renewable Raw Material to Obtain Bioproducts of High-Tech Value*; Popa, V., Volf, I., Ed.; Elsevier, 2018; Chapter 8, pp 271−313.

(17) Anjum, A.; Zuber, M.; Zia, K. M.; Noreen, A.; Anjum, M. N.; Tabasum, S. Microbial production of polyhydroxyalkanoates (PHAs) and its copolymers: A review of recent advancements. *Int. J. Biol. Macromol.* **2016**, *89*, 161−174.

(18) Brophy, M. R.; Deasy, P. B. B In vivo and in vitro studies on biodegradable polyester microparticles containing sulfamethizole. *Int. J. Pharm.* **1986**, *29*, 223−231.

(19) Gangrade, N.; Price, J. C. Poly(hydroxybutyrate-hydroxyvalerate) microspheres containing progesterone: preparation, morphology and release properties. *J. Microencapsulation* **1991**, *8*, 185−202.

(20) Gürsel, I.; Hasirci, V. Properties and drug release behaviour of poly(3-hydroxybutyric acid) and various poly(3-hydroxybutyrate-hydroxyvalerate) copolymer microcapsules. *J. Microencapsulation* **1995**, *12*, 185−193.

(21) Monnier, A.; Sheibat-Othman, N.; Chenal, J.-M.; Santos, A. M. d.; Fessi, H. Poly(hydroxybutyrate-co-hydroxyvalerate) Microspheres for the Encapsulation and Controlled Release of Heparin. *J. Colloid Sci. Biotechnol.* **2016**, *5*, 100−108.

(22) Peppas, N. A.; Brannon-Peppas, L. Controlled release of fragrances from polymers I. Thermodynamic analysis. *J. Controlled Release* **1996**, *40*, 245−250.

(23) Shmueli, R. B.; Ohnaka, M.; Miki, A.; Pandey, N. B.; Lima e Silva, R.; Koskimaki, J. E.; Kim, J.; Popel, A. S.; Campochiaro, P. A.; Green, J. J. Long-term suppression of ocular neovascularization by intraocular injection of biodegradable polymeric particles containing a serpin-derived peptide. *Biomaterials* **2013**, *34*, 7544−7551.

(24) Kirby, B. P.; Pabari, R.; Chen, C.-N.; Al Baharna, M.; Walsh, J.; Ramtoola, Z. Comparative evaluation of the degree of pegylation of poly(lactic-co-glycolic acid) nanoparticles in enhancing central nervous system delivery of loperamide. *J. Pharm. Pharmacol.* **2013**, *65*, 1473−1481.

(25) Larson, N.; Yang, J.; Ray, A.; Cheney, D. L.; Ghandehari, H.; Kopeček, J. Biodegradable multiblock poly(N-2-hydroxypropyl)-methacrylamide gemcitabine and paclitaxel conjugates for ovarian cancer cell combination treatment. *Int. J. Pharm.* **2013**, *454*, 435−443.

(26) Erdal, E.; Kavaz, D.; Şam, M.; Demirbilek, M.; Demirbilek, M. E.; Sağlam, N.; Denkbaş, E. B. Preparation and characterization of magnetically responsive bacterial polyester based nanospheres for cancer therapy. *J. Biomed. Nanotechnol.* **2012**, *8*, 800−808.

(27) Ma, Y.; Jiang, X.; Zhuo, R. Biodegradable and thermosensitive micelles of amphiphilic polyaspartamide derivatives containing

DOI: 10.1021/acsomega.9b00824
ACS Omega 2019, 4, 8122−8135

aromatic groups for drug delivery. *J. Polym. Sci., Part A: Polym. Chem.* **2013**, *51*, 3917−3924.
(28) Jaszcz, K.; Lukaszczyk, J.; Smiga-Matuszowicz, M. New biodegradable biomedical polymers based on succinic acid. *Polimery* **2013**, *58*, 670−677.
(29) Huang, C. L.; Steele, T. W.; Widjaja, E.; Boey, F. Y.; Venkatraman, S. S.; Loo, J. S. The influence of additives in modulating drug delivery and degradation of PLGA thin films. *NPG Asia Mater.* **2013**, *5*, No. e54.
(30) Takei, T.; Sugihara, K.; Yoshida, M.; Kawakami, K. Injectable and biodegradable sugar beet pectin/gelatin hydrogels for biomedical applications. *J. Biomater. Sci., Polym. Ed.* **2013**, *24*, 1333−1342.
(31) Marrache, S.; Pathak, R.; Darley, K.; Choi, J.; Zaver, D.; Kolishetti, N.; Dhar, S. Nanocarriers for Tracking and Treating Diseases. *Curr. Med. Chem.* **2013**, *20*, 3500−3514.
(32) Sinha, V. R.; Trehan, A. Biodegradable microspheres for protein delivery. *J. Controlled Release* **2003**, *90*, 261−280.
(33) Jelvehgari, M.; Montazam, S. Comparison of Microencapsulation by Emulsion-Solvent Extraction/Evaporation Technique Using Derivatives Cellulose and Acrylate-Methacrylate Copolymer as Carriers. *Jundishapur J. Nat. Pharm. Prod.* **2012**, *7*, 144−152.
(34) Fujiwara, M.; Shiokawa, K.; Kubota, T. Direct encapsulation of proteins into calcium silicate microparticles by water/oil/water interfacial reaction method and their responsive release behaviors. *Mater. Sci. Eng., C* **2012**, *32*, 2484−2490.
(35) Tiwari, S.; Verma, P. Microencapsulation technique by solvent evaporation method (Study of effect of process variables). *Int. J. Pharm. & Life Sci.* **2011**, *2*, 998−1005.
(36) Kilpatrick, P. K. Water-in-Crude Oil Emulsion Stabilization: Review and Unanswered Questions. *Energy Fuels* **2012**, *26*, 4017−4026.
(37) Tadros, T. Principles of Emulsion Stabilization with Special Reference to Polymeric Surfactants. *J. Cosmet. Sci.* **2006**, *57*, 153−169.
(38) Yoo, H. S. Preparation of biodegradable polymeric hollow microspheres using O/O/W emulsion stabilized by Labrafil. *Colloids Surf., B* **2006**, *52*, 47−51.
(39) Chen, C.; Yu, C. H.; Cheng, Y. C.; Yu, P. H. F.; Cheung, M. K. Preparation and characterization of biodegradable nanoparticles based on amphiphilic poly(3-hydroxybutyrate)−poly(ethylene glycol)−poly(3-hydroxybutyrate) triblock copolymer. *Eur. Polym. J.* **2006**, *42*, 2211−2220.
(40) Napper, D. H. Stabilization by attached polymer: steric stabilization, *Polymeric Stabilization of Colloidal Dispersions*; Academic Press: London, 1984; pp xviii+428.
(41) Zambaux, M.; Bonneaux, F.; Gref, R.; Maincent, P.; Dellacherie, E.; Alonso, M. J.; Labrude, P.; Vigneron, C. Influence of experimental parameters on the characteristics of poly(lactic acid) nanoparticles prepared by a double emulsion method. *J. Controlled Release* **1998**, *50*, 31−40.
(42) Müller, M.; Vörös, J.; Csúcs, G.; Walter, E.; Danuser, G.; Merkle, H. P.; Spencer, N. D. Surface modification of PLGA microspheres. *J. Biomed. Mater. Res., Part A* **2003**, *66*, 55−61.
(43) Woo, B. H.; Jiang, G.; Jo, Y. W.; DeLuca, P. P. Preparation and characterization of a composite PLGA and poly(acryloyl hydroxyethyl starch) microsphere system for protein delivery. *Pharm. Res.* **2001**, *18*, 1600−1606.
(44) Geiger, B. C.; Nelson, M. T.; Munj, H. R.; Tomasko, D. L.; Lannutti, J. J. Dual drug release from CO2-infused nanofibers via hydrophobic and hydrophilic interactions. *J. Appl. Polym. Sci.* **2015**, *132*, 42571.
(45) Kuo, C.-Y.; Liu, T.-Y.; Hardiansyah, A.; Lee, C.-F.; Wang, M.-S.; Chiu, W.-Y. Self-assembly behaviors of thermal- and pH- sensitive magnetic nanocarriers for stimuli-triggered release. *Nanoscale Res. Lett.* **2014**, *9*, 520.
(46) Mosaiab, T.; In, I.; Park, S. Y. Temperature and pH-Tunable Fluorescence Nanoplatform with Graphene Oxide and BODIPY-Conjugated Polymer for Cell Imaging and Therapy. *Macromol. Rapid Commun.* **2013**, *34*, 1408−1415.
(47) Leon, R. A. L.; Somasundar, A.; Badruddoza, A. Z. M.; Khan, S. A. Microfluidic fabrication of multi-drug-loaded polymeric microparticles for topical glaucoma therapy. *Part. Part. Syst. Charact.* **2015**, *32*, 567−572.
(48) Busatto, C.; Pesoa, J.; Helbling, I.; Luna, J.; Estenoz, D. Effect of particle size, polydispersity and polymer degradation on progesterone release from PLGA microparticles: Experimental and mathematical modeling. *Int. J. Pharm.* **2018**, *536*, 360−369.
(49) da Silva, A. R.; Zaniquelli, M. E. D.; Baratti, M. O.; Jorge, R. A. Drug Release from Microspheres and Nanospheres of Poly(lactide-co-glycolide) without Sphere Separation from the Release Medium. *J. Braz. Chem. Soc.* **2010**, *21*, 214−225.
(50) Herrán, E.; Pérez-González, R.; Igartua, M.; Pedraz, J. L.; Carro, E.; Hernández, R. M. VEGF-releasing biodegradable nanospheres administered by craniotomy: A novel therapeutic approach in the APP/Ps1 mouse model of Alzheimer's disease. *J. Controlled Release* **2013**, *170*, 111−119.
(51) Ganeshkumar, M.; Ponrasu, T.; Sathishkumar, M.; Suguna, L. Preparation of amphiphilic hollow carbon nanosphere loaded insulin for oral delivery. *Colloids Surf., B* **2013**, *103*, 238−243.
(52) Shen, Z.; Wu, A. Stealth contrast-enhancing material for early diagnosis of tumors and preparation method thereof. China Patent CN102743768 A, July 03, 2012.
(53) Banerjee, R.; Thanigaivel, S.; Chakravarty, S.. A nanocochelate-nanosphere complex. Indian Patent 2190/MUM/2011, Aug 02, 2011.
(54) Eke, G.; Kuzmina, A. M.; Goreva, A. V.; Shishatskaya, E. I.; Hasirci, N.; Hasirci, V. In vitro and transdermal penetration of PHBV micro/nanoparticles. *J. Mater. Sci.: Mater. Med.* **2014**, *25*, 1471−1481.
(55) Mekala, M.; Rajendran, R. Nano encapsulation with interfacial deposition of PHB (Poly −B- Hydroxybutrate) as nanparticle with amphicilin. *Int. J. Recent Sci. Res.* **2016**, *7*, 9156−9160.
(56) Cutts, L. S.; Hibberd, S.; Adler, J.; Davies, M. C.; Melia, C. D. Characterising drug release processes within controlled release dosage forms using the confocal laser scanning microscope. *J. Controlled Release* **1996**, *42*, 115−124.
(57) Meyvis, T. K. L.; De Smedt, S. C.; Van Oostveldt, P.; Demeester, J. Fluorescence recovery after photobleaching: a versatile tool for mobility and interaction measurements in pharmaceutical research. *Pharm. Res.* **1999**, *16*, 1152−1162.
(58) Shrivastav, A.; Kim, H.-Y.; Kim, Y.-R. Advances in the Applications of Polyhydroxyalkanoate Nanoparticles for Novel Drug Delivery System. *BioMed Res. Int.* **2013**, *2013*, 581684.
(59) Shah, M.; Ullah, N.; Choi, M. H.; Kim, M. O.; Yoon, S. C. Amorphous amphiphilic P(3HV-co-4HB)-b-mPEG block copolymer synthesized from bacterial copolyester via melt transesterification: nanoparticle preparation, cisplatin-loading for cancer therapy and in vitro evaluation. *Eur. J. Pharm. Biopharm.* **2012**, *80*, 518−527.
(60) Lira, R. A.; Myamoto, D. M.; Souza, J. R.; Nascimento, N.; Junior, J. A. O.; Martinelli, J. R.; Azevedo, M. B. M. Microspheres with ultra high holmium content for brachytherapy of malignancies. *2011 International Nuclear Atlantic Conference—INAC 2011*; Associação Brasileira de Energia Nuclear— ABEN: Belo Horizonte, MG, Brazil, Oct 24−28, 2011.
(61) Lamprecht, A.; Schäfer, U. F.; Lehr, C.-M. Characterization of microcapsules by confocal laser scanning microscopy: structure, capsule wall composition and encapsulation rate. *Eur. J. Pharm. Biopharm.* **2000**, *49*, 1−9.
(62) Caponetti, G.; Hrkach, J. S.; Kriwet, B.; Poh, M.; Lotan, N.; Colombo, P.; Langer, R. Microparticles of novel branched copolymers of lactic acid and amino acids: preparation and characterization. *J. Pharm. Sci.* **1999**, *88*, 136−141.
(63) Nie, S.; Chiu, D.; Zare, R. Probing individual molecules with confocal fluorescence microscopy. *Science* **1994**, *266*, 1018−1021.
(64) Embleton, J. K.; Tighe, B. J. Polymers for biodegradable medical devices XI. Microencapsulation studies: characterization of hydrocortisone-loaded poly-hydroxybutyrate-hydroxyvalerate microspheres. *J. Microencapsulation* **2002**, *19*, 737−752.

DOI: 10.1021/acsomega.9b00824
ACS Omega 2019, 4, 8122−8135

(65) Martin, M. A.; Miguens, F. C.; Rieumont, J.; Sanchez, R. Tailoring of the external and internal morphology of poly-3-hydroxy butyrate microparticles. *Colloids Surf., B* **2000**, *17*, 111−116.
(66) Šics, I.; Ezquerra, T. A.; Nogales, A.; Balta-Calleja, F. J.; Kalnins, M.; Tupureina, V. On the Relationship between Crystalline Structure and Amorphous Phase Dynamics during Isothermal Crystallization of Bacterial Poly(3-hydroxybutyrate-co-3-hydroxyvalerate) Copolymers. *Biomacromolecules* **2001**, *2*, 581−587.
(67) Owen, A. J.; Heinzel, J.; Škrbić, Ž.; Divjaković, V. Crystallization and melting behaviour of PHB and PHB/HV copolymer. *Polymer* **1992**, *33*, 1563−1567.
(68) Barham, P.; Barker, P.; Organ, S. J. Physical properties of poly(hydroxybutyrate) and copolymers of hydroxybutyrate and hydroxyvalerate. *FEMS Microbiol. Rev.* **1992**, *103*, 289−298.
(69) Yoshie, N.; Saito, M.; Inoue, Y. Effect of chemical compositional distribution on solid-state structures and properties of poly(3-hydroxybutyrate-co-3-hydroxyvalerate). *Polymer* **2004**, *45*, 1903−1911.
(70) de Almeida Neto, G. R.; Barcelos, M. V.; Almeida, F. M.; Rodriguez, R. J. S.; Gomez, J. G. C. Influence of Encapsulated Nanodiamond Dispersion on P(3HB) Biocomposites Properties. *Mater. Res.* **2017**, *20*, 768−774.
(71) Dzyaloshinskii, I. E.; Lifshitz, E. M.; Pitaevskii, L. P. General theory of van der Waals' forces. *Sov. Phys. Uspekhi* **1961**, *4*, 153−176.
(72) Murakami, H.; Kawashima, Y.; Niwa, T.; Hino, T.; Takeuchi, H.; Kobayashi, M. Influence of the degrees of hydrolyzation and polymerization of poly(vinylalcohol) on the preparation and properties of poly(dl-lactide-co-glycolide) nanoparticle. *Int. J. Pharm.* **1997**, *149*, 43−49.
(73) Mu, L.; Feng, S.-S. PLGA/TPGS Nanoparticles for controlled release of Paclitaxel: effects of the emulsifier and drug loading ratio. *Pharm. Res.* **2003**, *20*, 1864−1872.
(74) Lee, S. C.; Oh, J. T.; Jang, M. H.; Chung, S. I. Quantitative analysis of polyvinyl alcohol on the surface of poly(D,L-lactideco-glycolide) microparticles prepared by solvent evaporation method: effect of particle size and PVA concentration. *J. Controlled Release* **1999**, *59*, 123−132.
(75) Mu, L.; Feng, S. S. A novel controlled release formulation for the anticancer drug paclitaxel (Taxol): PLGA nanoparticles containing vitamin E TPGS. *J. Controlled Release* **2003**, *86*, 33−48.
(76) Tiwari, V. K.; Singh, N. K.; Avasthi, D. K.; Misra, M.; Maiti, P. Swift heavy ions induced controlled biodegradation of poly(ε-caprolactone) nanohybrids. *Radiat. Phys. Chem.* **2013**, *82*, 92−99.
(77) Zonari, A.; Novikoff, S.; Electo, N. R. P.; Breyner, N. M.; Gomes, D. A.; Martins, A.; Neves, N. M.; Reis, R. L.; Goes, A. M. Endothelial differentiation of human stem cells seeded onto electrospun polyhydroxybutyrate/polyhydroxybutyrate-co-hydroxyvalerate fiber mesh. *PLoS One* **2012**, *7*, No. e35422.
(78) Renard, E.; Vergnol, G.; Langlois, V. Adhesion and proliferation of human bladder RT112 cells on functionalized polyesters. *IRBM* **2011**, *32*, 214−220.
(79) Choi, W. M.; Kim, T. W.; Park, O. O.; Chang, Y. K.; Lee, J. W. Preparation and characterization of poly(hydroxybutyrate-co-hydroxyvalerate)−organoclay nanocomposites. *J. Appl. Polym. Sci.* **2003**, *90*, 525−529.
(80) Yu, C.-L.; Bian, F.; Zhang, S.-F.; Xu, X.; Ren, P.; Wang, F.-C.; Zhang, F.-A. Preparation of the monodispersed carboxyl-functionalized polymer microspheres with disproportionated rosin moiety and adsorption of methylene blue. *Adsorpt. Sci. Technol.* **2018**, *36*, 1260−1273.
(81) Ford, R. A.; Hawkins, D. R.; Mayo, B. C.; Api, A. M. The in vivo dermal absorption and metabolism of [4-14C]coumarin by rats and by human volunteers under simulated conditions of use in fragrances. *Food Chem. Toxicol.* **2001**, *39*, 153−162.
(82) Atanase, L. I.; Bistac, S.; Riess, G. Effect of poly(vinyl alcohol-co-vinyl acetate) copolymer blockiness on the dynamic interfacial tension and dilational viscoelasticity of polymer−anionic surfactant complex at the water−1-chlorobutane interface. *Soft Matter* **2015**, *11*, 2665−2672.
(83) Atanase, L.; Riess, G. Thermal Cloud Point Fractionation of Poly(vinyl alcohol-co-vinyl acetate): Partition of Nanogels in the Fractions. *Polymers* **2011**, *3*, 1065−1075.
(84) Atanase, L. I.; Riess, G. Poly(vinyl alcohol-co-vinyl acetate) complex formation with anionic surfactants particle size of nanogels and their disaggregation with sodium dodecyl sulfate. *Colloids Surf., A* **2010**, *355*, 29−36.
(85) Tian, F.; Zhao, Y. L.; Liu, C. J.; Li, F.; Xing, N. The vitro and vivo study of Poly(3-hydroxybutyrate)microspheres. In *7th Asian-Pacific Conference on Medical and Biological Engineering APCMBE 2008, IFMBE Proceedings 19*; Peng, Y., Weng, X., Eds.; Spring-Verlag Berlim Heidelberg, 2008; pp 615−622.
(86) Murakami, H.; Kobayashi, M.; Takeuchi, H.; Kawashima, Y. Preparation of poly(DL-lactide-co-glycolide) nanoparticles by modified spontaneous emulsification solvent diffusion method. *Int. J. Pharm.* **1999**, *187*, 143−152.
(87) Thies, C. Complex coacervation. In *How to Make Microcapsules—Lecture and Laboratory Manual*; Thies, C., Ed.; Thies Technology: Saint Louis, Missouri, 1995; Chapter 5, pp 1−43.
(88) Sahoo, S. K.; Panyam, J.; Prabha, S.; Labhasetwar, V. Residual polyvinyl alcohol associated with poly (D,L-lactide-co-glycolide) nanoparticles affects their physical properties and cellular uptake. *J. Controlled Release* **2002**, *82*, 105−114.
(89) Lamprecht, A.; Schäfer, U.; Lehr, C.-M. Structural analysis of microparticles by confocal laser scanning microscopy. *AAPS PharmSciTech* **2000**, *1*, 10−19.
(90) Ruan, G.; Feng, S.-S.; Li, Q.-T. Effects of material hydrophobicity on physical properties of polymeric microspheres formed by double emulsion process. *J. Controlled Release* **2002**, *84*, 151−160.
(91) Image Tool http://ddsdx.uthscsa.edu/dig/itdesc.html (2004) (accessed and downloaded March 2007).
(92) Joshi, D. P.; Lan-Chun-Fung, Y. L.; Pritchard, J. G. Determination of poly(vinyl alcohol) via its complex with boric acid and iodine. *Anal. Chim. Acta* **1979**, *104*, 153−160.

DOI: 10.1021/acsomega.9b00824
ACS Omega 2019, 4, 8122−8135